J Math Chem (2011) 49:1961–1975
DOI 10.1007/s10910-011-9867-7

ORIGINAL PAPER

The two-body problem with generalized Lennard-Jones potential

Mihail Bărbosu · Vasile Mioc · Daniel Paşca · Ferenc Szenkovits

Received: 12 May 2011 / Accepted: 13 June 2011 / Published online: 26 June 2011

Abstract We consider a generalization of the famous Lennard-Jones potential. To study the two-body problem associated to this potential, we use the foliations of the phase space by the invariant sets corresponding to the first integrals of energy and angular momentum. We investigate all possible situations created by the interplay among the constants of integration and the field parameters. We obtain the global flow, and illustrate it in both 3D and 2D. This flow exhibits a great variety of orbits, a homoclinic one included. All phase portraits are interpreted in terms of physical trajectories.

Keywords Dynamical systems · Topology · Lennard-Jones model · Motion in a potential field · Global flow

M. Bărbosu
Department of Mathematics, The College at Brockport, State University of New York, 350 New Campus Dr. Brockport, Brockport, NY 14420, USA
e-mail: mbarbosu@brockport.edu

V. Mioc
Astronomical Institute of the Romanian Academy, Str. Cuţitul de Argint 5, Bucharest 040557, Romania
e-mail: vmioc@aira.astro.ro

D. Paşca (✉)
Department of Mathematics and Informatics, University of Oradea, University Street 1, Oradea 410087, Romania
e-mail: dpasca@uoradea.ro

F. Szenkovits
Department of Applied Mathematics, Babeş-Bolyai University, Str. Mihail Kogalniceanu 1, Cluj-Napoca 400084, Romania
e-mail: fszenko@math.ubbcluj.ro

1 Introduction

The Lennard-Jones potential (see [3]) is a very famous empirical function in molecular dynamics. It models the interaction between two neutral atoms or molecules, which are subject to two distinct forces in the limit of large separation and small separation. These are: an attractive force at long ranges (van der Waals force, or dispersion force), and a repelling force at short ranges (result of overlapping electron orbitals, referred to as Pauli repulsion from Pauli's exclusion principle).

This potential (also called 6–12 potential or 12–6 potential) reads $U_{LJ} = 4\epsilon\left[(\sigma/r)^6 - (\sigma/r)^{12}\right]$, where: ϵ = depth of the potential energy well; σ = finite distance at which the interparticle potential is zero; r = distance between the two particles. These parameters can be fitted to reproduce experimental data, or can be deduced from results of accurate quantum chemistry calculations.

The Lennard-Jones potential is an empirical approximation. The form of the repulsion term, in $(1/r)^{12}$, has no theoretical substantiation. Actually, the repelling force should depend exponentially on the distance. But the repulsion term in the Lennard-Jones formula is more convenient due to the ease and efficiency of computing the square of $(1/r)^6$. It physically originates in Pauli's principle, but the exponent 12 was chosen exclusively because of ease of computation. As to the attractive long-range potential, it is derived from dispersion interactions.

Even if it is an empirical model, the Lennard-Jones potential proved itself to be a relatively good approximation. It is often used to describe the properties of gases, and to model dispersion and overlap interactions in molecular models. Moreover, an extension of this model was used to study some special combinations of concrete astronomical situations (see [6,7]).

The problem we approach and fully answer in this paper is the two-body problem associated to a generalized Lennard-Jones-type potential of the form $A/r^a - B/r^b$. It is clear that this type of potential covers much more physical situations than the original Lennard-Jones one. We have to point out the fact that we are interested here only in the mathematical aspects of the dynamics and not in the concrete physical ones.

Section 2 points out the basic equations of the problem, reduced to a central-force problem. We write the Hamiltonian equations of motion in polar coordinates, and we specify the conditions for the potential parameters. Then we emphasize the first integrals that characterize the problem: the energy integral and the angular momentum integral. Lastly, we present the algorithm of foliations intended to depict the phase space.

The very short Sect. 3 defines the critical values of the Hamiltonian equations of motion.

In Sect. 4 we introduce the Hill regions of the configuration space, where all solutions with the same energy are lying. We differentiate the situations positive/zero/negative energy, and we point out the diffeomorphisms between the Hill region and various algebraic sets.

Section 5 computes the energy levels in a direct way. The topology of the constant-energy set is established according to the values of the energy constant and field parameters. In Sect. 6 we use another way to compute the energy levels, which allows

us to examine the foliation of the constant-energy set by the constant-angular-momentum set. All the topological equivalents are presented in tabular form.

In Sect. 7 we present some 3D phase portraits of the situations we have investigated.

In Sect. 8 we give the interpretation of the topological types presented tabularly in Sect. 6 in terms of 2D orbits in the phase plane (r, x) (x being the equivalent of p_r after a Sundman-type transformation). All phase curves are translated in terms of physical orbits.

Section 9 formulates some concluding remarks.

2 Basic equations

In this paper we study the global phase portrait of the generalized Lennard-Jones potential

$$V(r) = \frac{A}{r^a} - \frac{B}{r^b}$$

with $b > a > 2$ and $A > 0$, $B > 0$, using its formulation as an integrable Hamiltonian system with two degrees of freedom. More precisely, in polar coordinates (r, θ) for the position and (p_r, p_θ) for the momenta, the Hamiltonian which governs the generalized Lennard-Jones systems is

$$H = \frac{1}{2}\left(p_r^2 + \frac{p_\theta^2}{r^2}\right) - \frac{A}{r^a} + \frac{B}{r^b}. \tag{1}$$

Its Hamiltonian system is

$$\dot{r} = \frac{\partial H}{\partial p_r}, \quad \dot{\theta} = \frac{\partial H}{\partial p_\theta}, \quad \dot{p}_r = -\frac{\partial H}{\partial r}, \quad \dot{p}_\theta = -\frac{\partial H}{\partial \theta} = 0. \tag{2}$$

Then, the Hamiltonian H and the angular momentum p_θ are two first integrals, independent and in involution. Hence, the Hamiltonian system (2) is integrable.

If we denote by $\mathbf{R}^+$ the open interval $(0, \infty)$, then the generalized Lennard-Jones system *phase space* is $E = \mathbf{R}^+ \times \mathbf{S}^1 \times \mathbf{R}^2$ where $r \in \mathbf{R}^+$, $\theta \in \mathbf{S}^1$ and $(p_r, p_\theta) \in \mathbf{R}^2$. Since H and p_θ are first integrals, the sets

$$\begin{aligned} I_h &= \{(r, \theta, p_r, p_\theta) \in E \ : \ H(r, \theta, p_r, p_\theta) = h\}, \\ I_c &= \{(r, \theta, p_r, p_\theta) \in E \ : \ p_\theta = c\}, \\ I_{hc} &= I_h \cap I_c, \end{aligned}$$

are invariant by the Hamiltonian flow of (2).

The main results of this paper are the description of the foliations of

(i) the phase space E by the invariant sets I_h,
(ii) I_h by the invariant sets I_{hc}, and
(iii) I_{hc} by the flow of the Hamiltonian system.

These foliations provide a good description of the phase portraits of the Hamiltonian flows defined by (2) when a, b, A and B vary.

3 Critical values of H

A point $(r, \theta, p_r, p_\theta) \in E$ is *critical* for the map $H: E \to \mathbf{R}$ if it is a solution of the system

$$\frac{\partial H}{\partial r} = 0, \quad \frac{\partial H}{\partial \theta} = 0, \quad \frac{\partial H}{\partial p_r} = 0, \quad \frac{\partial H}{\partial p_\theta} = 0. \tag{3}$$

The value $h \in \mathbf{R}$ is *critical* for the map $H: E \to \mathbf{R}$ if there is some critical point belonging to $H^{-1}(h) = I_h$. If $h \in \mathbf{R}$ is not critical, then h is a *regular* value. It is well known that if h is a regular value of the map $H: E \to \mathbf{R}$, then I_h is a three-dimensional manifold (see for instance [2]).

Since $r > 0$ system (3) reduces to

$$r = \left(\frac{Bb}{Aa}\right)^{\frac{1}{b-a}} \qquad p_r = p_\theta = 0$$

and the set of critical points of H is

$$\mathcal{C} = \left\{\left(\left(\frac{Bb}{Aa}\right)^{\frac{1}{b-a}}, \theta, 0, 0\right) : \theta \in \mathbf{S}^1\right\}.$$

4 Hill regions

Let $\pi: E \to \mathbf{R}^+ \times \mathbf{S}^1$ be the natural projection from the phase space E to the *configuration space* $\mathbf{R}^+ \times \mathbf{S}^1$. Then for each $h \in \mathbf{R}$, the *Hill region* R_h of I_h is defined by $R_h = \pi(I_h)$. Therefore

$$\begin{aligned} R_h &= \left\{(r, \theta) \in \mathbf{R}^+ \times \mathbf{S}^1 \ : \ -\frac{A}{r^a} + \frac{B}{r^b} \le h\right\} \\ &\approx \{r \in \mathbf{R}^+ \ : \ r^b h + r^{b-a} A - B \ge 0\} \times \mathbf{S}^1 \end{aligned} \tag{4}$$

where, as usual, $\approx$ means "diffeomorphic to". Note that the Hill region R_h is the region of the configuration space or position space where the motion of all orbits having energy h takes place. We denote $f(r) = hr^b + Ar^{b-a} - B$.

- If $h > 0$ there exists a unique $r_h > 0$ such that $f(r_h) = 0$, and R_h is diffeomorphic to $[r_h, \infty) \times \mathbf{S}^1$.
- If $h = 0$ then R_h is diffeomorphic to $[(B/A)^{1/(b-a)}, \infty) \times \mathbf{S}^1$.

- If $h < 0$ there exists a unique

$$r_c = \left(-\frac{A(b-a)}{hb}\right)^{1/a} \text{ such that } f'(r_c) = 0,$$

and

$$f(r_c) = \frac{(-h)^{1-b/a}}{\frac{b}{a}-1}\left[A\left(1-\frac{a}{b}\right)\right]^{b/a} - B.$$

Let us denote

$$h^* = -\left\{\frac{B(b/a-1)}{[A(1-a/b)]^{b/a}}\right\}^{a/(a-b)},$$

then,

* if $h < h^*$ then $f(r_c) > 0$ which implies that there exist $r_1^* < r_2^*$ such that $f(r_i^*) = 0$ and hence R_h is diffeomorphic to $[r_1^*, r_2^*] \times \mathbf{S}^1$.
* if $h = h^*$ then $f(r_c) = 0$ and hence R_h is diffeomorphic to $\{r_c\} \times \mathbf{S}^1$.
* if $h > h^*$ then $f(r_c) < 0$ and hence R_h is diffeomorphic to $\emptyset$.

5 Energy levels I_h

We compute the energy levels I_h in two different ways. The first way, described in this section, is more direct. The second way, described in the next section, allows one to additionally deduce the foliation of I_h by the invariant sets I_{hc}.

From the definition of I_h we have

$$I_h = \bigcup_{(r,\theta)\in R_h} E_{(r,\theta)} \tag{5}$$

where

$$E_{(r,\theta)} = \left\{(r, \theta, p_r, p_\theta) \in E \ : \ p_r^2 + \frac{p_\theta^2}{r^2} = \frac{2}{r^b}(hr^b + Ar^{b-a} - B)\right\}.$$

Clearly, for each (r, θ) given, the set $E_{(r,\theta)}$ is an ellipse, a point, or the empty set, if the point (r, θ) belongs to the interior of R_h, to the boundary of R_h, or does not belong to R_h, respectively. Therefore, from (5), the previous section and some topology, the topology of I_h easily follows according to the different values of h, a, b, A and B.

If $h \geq 0$, then I_h is diffeomorphic to $\mathbf{S}^3 \setminus \mathbf{S}^1$, which is also diffeomorphic to an open solid torus $\mathbf{T}^3$ of $\mathbf{R}^3$.

If $h \in (h^*, 0)$, then I_h is diffeomorphic to $\emptyset$.

If $h = h^*$, then I_h is diffeomorphic to $\mathbf{S}^1$.

If $h \in (-\infty, h^*)$, then I_h is diffeomorphic to $\mathbf{S}^3$.

6 Invariant sets I_{hc}

In this section we first compute again the invariant energy levels I_h, but now using the fact that

$$I_h = \{(r, \theta, p_r, p_\theta) \in E \ : \ g(r, p_r, p_\theta) = h\} \approx g^{-1}(h) \times \mathbf{S}^1 \tag{6}$$

where

$$g(r, p_r, p_\theta) = \frac{1}{2}\left(p_r^2 + \frac{p_\theta^2}{r^2}\right) - \frac{A}{r^a} + \frac{B}{r^b}.$$

If $h \in \mathbf{R}$ is a regular value of the map $g: \mathbf{R}^+ \times \mathbf{R}^2 \to \mathbf{R}$ and $g^{-1}(h) \neq \emptyset$, then $g^{-1}(h)$ is a surface of $\mathbf{R}^+ \times \mathbf{R}^2$. It is easy to verify that the intersection of $g^{-1}(h)$ with $\{r = r_0 = \text{constant}\}$, is an ellipse, a point, or the empty set according to whether $hr_0^b + Ar_0^{b-a} - B$ is positive, zero, or negative, respectively. So, by studying the union of the ellipses or points of the form $g^{-1}(h) \cap \{r = r_0\}$ while $r_0 > 0$ varies, we obtain the sets $g^{-1}(h)$. Therefore, from (6), we calculate in a different way (with respect to the previous section) the topology of the energy levels I_h.

We note that knowing the sets $g^{-1}(h)$, from

$$I_{hc} = I_h \cap \{p_\theta = c\} \approx \left(g^{-1}(h) \cap \{p_\theta = c\}\right) \times \mathbf{S}^1 \tag{7}$$

we can compute the invariant sets I_{hc}. Consequently, we can describe the foliation of I_h by I_{hc} when h varies. For this, we use the effective potential

$$V_c : (0, \infty) \longrightarrow \mathbf{R}, \quad V_c(r) = \frac{c^2}{2r^2} - \frac{A}{r^a} + \frac{B}{r^b},$$

and its derivative

$$V_c'(r) = -\frac{c^2}{r^3} + \frac{aA}{r^{a+1}} - \frac{bB}{r^{b+1}}.$$

Conditions	Topological type of I_{hc}	
C_1		
$h \leq 0$	$\varnothing$	–
$h > 0$	$\mathbf{S}^1 \times \mathbf{R}$	Cylinder
C_2		
$h \leq 0$	$\varnothing$	–
$h \in (0, V_c(r_1)) \cup (V_c(r_2), \infty)$	$\mathbf{S}^1 \times \mathbf{R}$	Cylinder
$h = V_c(r_1)$	$\mathbf{S}^1 \cup \left(\mathbf{S}^1 \times \mathbf{R}\right)$	Disjoint union of circle and cylinder

Table continued

$h \in (V_c(r_1), V_c(r_2))$	$\left(\mathbf{S}^1 \times \mathbf{S}^1\right) \cup \left(\mathbf{S}^1 \times \mathbf{R}\right)$	Disjoint union of
	$\left(\mathbf{S}^1 \times \mathbf{S}^1\right) \cap \left(\mathbf{S}^1 \times \mathbf{R}\right) = \varnothing$	torus and cylinder
$h = V_c(r_2)$	$\left(\mathbf{S}^1 \times \mathbf{S}^1\right) \cup \left(\mathbf{S}^1 \times \mathbf{R}\right)$	Union of torus and cylinder
	$\left(\mathbf{S}^1 \times \mathbf{S}^1\right) \cap \left(\mathbf{S}^1 \times \mathbf{R}\right) = \mathbf{S}^1$	with a common circle
C_3		
$h < 0$	$\varnothing$	
$h = 0$	$\mathbf{S}^1$	Circle
$h \in (0, V_c(r_2))$	$\left(\mathbf{S}^1 \times \mathbf{S}^1\right) \cup \left(\mathbf{S}^1 \times \mathbf{R}\right)$	Disjoint union of
	$\left(\mathbf{S}^1 \times \mathbf{S}^1\right) \cap \left(\mathbf{S}^1 \times \mathbf{R}\right) = \varnothing$	Circle and cylinder
$h = V_c(r_2)$	$\left(\mathbf{S}^1 \times \mathbf{S}^1\right) \cup \left(\mathbf{S}^1 \times \mathbf{R}\right)$	Union of torus and cylinder
	$\left(\mathbf{S}^1 \times \mathbf{S}^1\right) \cap \left(\mathbf{S}^1 \times \mathbf{R}\right) = \mathbf{S}^1$	with a common Circle
$h > V_c(r_2)$	$\mathbf{S}^1 \times \mathbf{R}$	Cylinder
C_4		
$h < V_c(r_1) < 0$	$\varnothing$	–
$h = V_c(r_1)$	$\mathbf{S}^1$	Circle
$h \in (V_c(r_1), 0]$	$\mathbf{S}^1 \times \mathbf{S}^1$	Torus
$h \in (0, V_c(r_2))$	$\left(\mathbf{S}^1 \times \mathbf{S}^1\right) \cup \left(\mathbf{S}^1 \times \mathbf{R}\right)$	Disjoint union of
	$\left(\mathbf{S}^1 \times \mathbf{S}^1\right) \cap \left(\mathbf{S}^1 \times \mathbf{R}\right) = \varnothing$	torus and cylinder
$h = V_c(r_2)$	$\left(\mathbf{S}^1 \times \mathbf{S}^1\right) \cup \left(\mathbf{S}^1 \times \mathbf{R}\right)$	Union of torus and cylinder
	$\left(\mathbf{S}^1 \times \mathbf{S}^1\right) \cap \left(\mathbf{S}^1 \times \mathbf{R}\right) = \mathbf{S}^1$	with a common circle
$h > V_c(r_2)$	$\mathbf{S}^1 \times \mathbf{R}$	Cylinder

Conditions: $C_1 \Longleftrightarrow V_c'(r) \leq 0, \forall r \in (0,\infty) \Longleftrightarrow c^2 r^{b-2} - aAr^{b-a} + bB \geq 0, \forall r \in (0,\infty)$; $C_2 \Longleftrightarrow \exists r_1, r_2, 0 < r_1 < r_2 : V_c'(r_1) = V_c'(r_2) = 0$ and $V_c(r_1) > 0$; $C_3 \Longleftrightarrow \exists r_1, r_2, 0 < r_1 < r_2 : V_c'(r_1) = V_c'(r_2) = 0$ and $V_c(r_1) = 0$; $C_4 \Longleftrightarrow \exists r_1, r_2, 0 < r_1 < r_2 : V_c'(r_1) = V_c'(r_2) = 0$ and $V_c(r_1) < 0$.

7 3D Phase portraits

This section deals with the 3D surfaces generated by the function $g^{-1}(h)$. Although the choice of the parameters A, a, B and b of the Lennard-Jones potential as well as the angular momentum constant c lead to different forms of $g^{-1}(h)$, we selected one representative plot for each class of similar topological surfaces. The 3D plots will be presented in connection with the table from Sect. 6 and the 2D phase portraits from Sect. 8, considering different values of the constant of energy, as $h < 0, h = 0$ and $h > 0$, respectively.

Case 1: $h < 0$ and $h = 0$.

For $h < 0$ and $h = 0$, one obvious sub-case is the one where the plot of $g^{-1}(h)$ is $\emptyset$. Basically, the left-hand side of Eq. (6), $g(r, p_r, p_\theta)$ is positive, while the right-hand side, h, is negative or zero. This corresponds to the first two lines of C_1, C_2 and to the first lines of C_3 and C_4 of the previous table.

When $h = V_c(r_1) < 0$, the equation for $g^{-1}(h)$ is reduced to $p_r^2 = 0$, and I_{hc} is a circle (line 2 of C_4 and point SE in Sect. 8). This also happens when $h = V_c(r_1) = 0$ (line 2 of C_3 and point SE in Sect. 8).

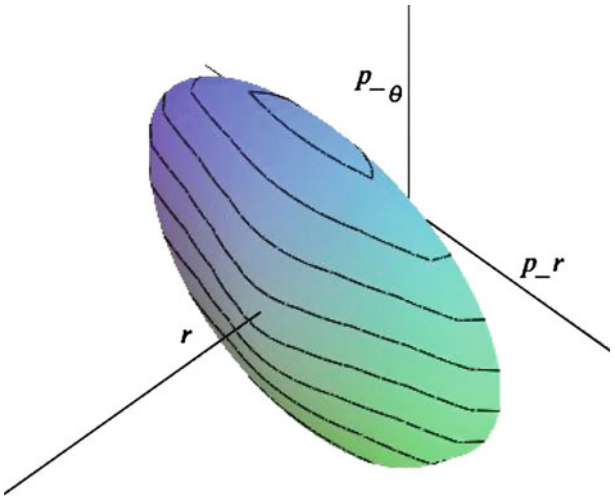

Fig. 1 The surface $g^{-1}(h)$ for $h \in (V_c(r_1), 0]$ and condition C_4

Figure 1 exemplifies the third line of C_4, with $h \in (V_c(r_1), 0]$ and we see that the surface of $g^{-1}(h)$ is homeomorphic to a sphere $\mathbf{S}^2$. The interpretation of the I_{hc} curves is given in Sect. 8.

Case 2: $h > 0$.
For $h > 0$ there is a variety of phase portraits.

We start with the surface corresponding to the second line of C_1 and to the type-4 orbits of Sect. 8, which are homeomorphic to $\mathbf{R}$. The surface of $g^{-1}(h)$ is the topological plane given in Fig. 2. In order to emphasize the connection between the table from Sect. 6 and the orbits of Sect. 8, in what follows we will focus on the top of the $g^{-1}(h)$ surfaces (obtained for positive values of the angular momentum) and on the level curves on these surfaces. This way, for Fig. 2, we get Fig. 3; note that for negative values of c, we obtain a surface symmetric with respect to the (r, p_r) plane.

Similar surfaces to the ones in Fig. 3 are obtained for conditions C_3-line 5 and C_4-line 6; the orbits are type-4 orbits. Next we consider the surface in Fig. 4 (again for $c > 0$) which has two components: a topological plane and a sphere. The orbits matching these surfaces are the type-3 and the type-4 orbits (for larger values of r) in the phase portrait.

A particular case of the one described in Fig. 4 matches conditions C_2 -line 3, when the component closer to the origin, is reduced to a point. This is the SE point in the phase portrait.

From Fig. 4 - type surfaces, if the energy h increases, the two components get closer until they share a common circle, in Fig. 5, or, for $c > 0$ in Fig. 6. The phase portrait contains now the previous type-3 and type-4 orbits, but also the type-2 curves, the homoclinic curve, H, and the type-1 orbits.

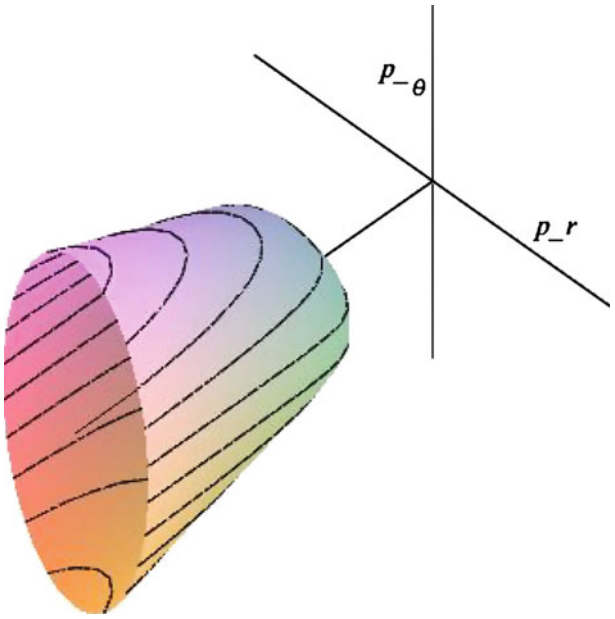

Fig. 2 The surface $g^{-1}(h)$ for $h > 0$ and condition C_1

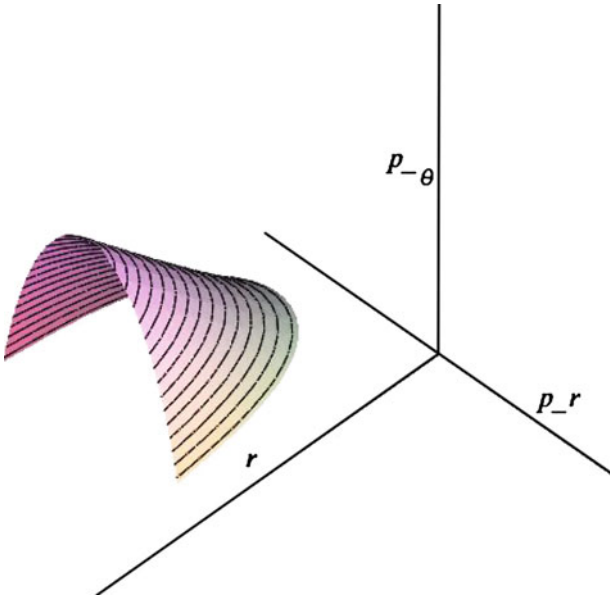

Fig. 3 The surface $g^{-1}(h)$ and level curves for Fig. 2, and $c > 0$

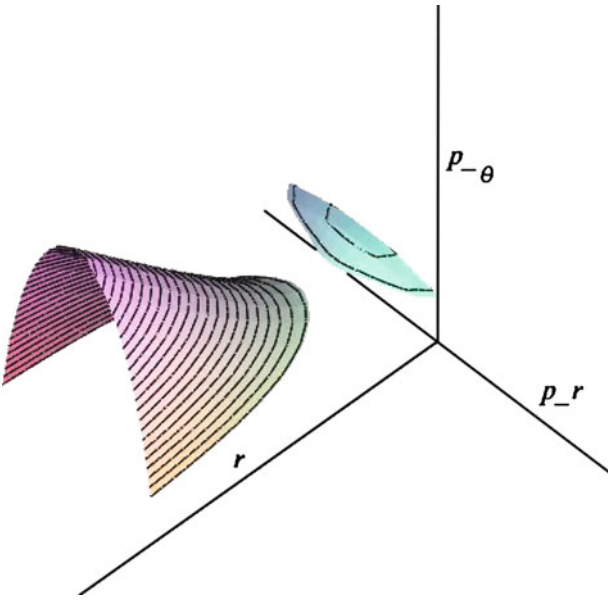

Fig. 4 The surface $g^{-1}(h)$ and level curves for conditions C_2-line 4, C_3-line 3 or C_4-line 4, and $c > 0$

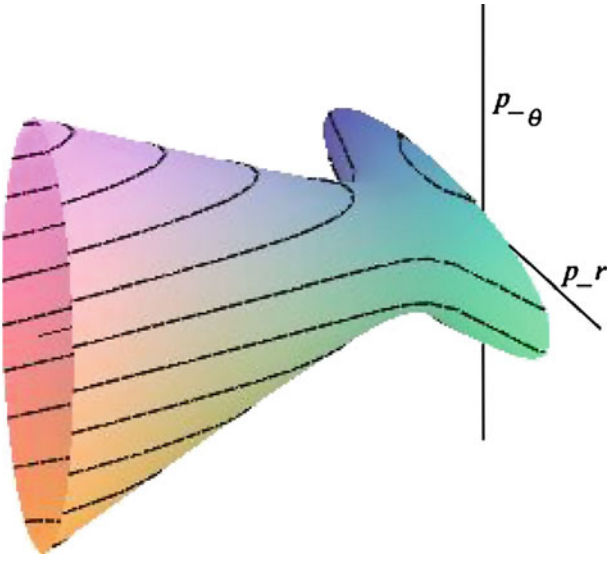

Fig. 5 The surface $g^{-1}(h)$ for conditions C_2-line 5, C_3-line 4 or C_4-line 5, and $c > 0$

In analyzing the role of the 4 parameters, A and B, a and b, in the Lennard-Jones potential, two sub-cases stand out, as A and B are comparable or when one of them is much larger than the other one. Nevertheless, the $g^{-1}(h)$ surfaces are topologically equivalent to the ones described above and don't lead to new cases.

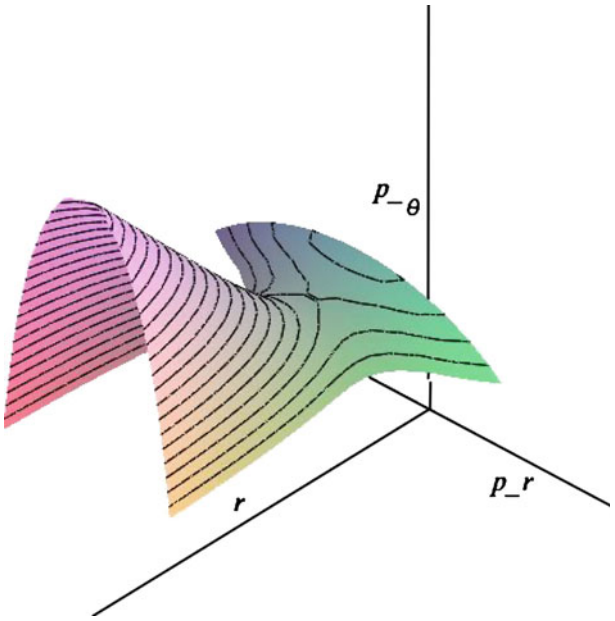

Fig. 6 The surface $g^{-1}(h)$ and level curves for Fig. 5 surfaces, and $c > 0$

8 2D Phase portraits and physical orbits

It is clear that our potential is central (the motion is planar and the two-body problem was already reduced to a central-force problem, see Sect. 2). It is also clear that in our model collisions between particles cannot occur. This was proved by Saari (see [8]) or Mioc and Stavinschi (see [5]) within different contexts.

Let us translate the topological types of I_{hc} in terms of phase orbits in the plane (r, x) (x being the equivalent of p_r after a Sundman-type transformation via a McGehee-type transformation (see [4] or [6]). The 2D phase portraits are given in Figs. 7, 8, and 9 below. According to the table in Sect. 6, we state the following equivalences:

- cylinder = unbounded phase orbits that come from infinity and then tend back to infinity (curves 2 in Fig. 8, 1 in Fig. 9).
- torus = quasiperiodic or periodic phase orbits (curves 1 in Fig. 7 and 3 in Fig. 9).
- circle = phase equilibrium (centre SE in Fig. 7 and Fig. 9, and saddle UE in Fig. 9).
- disjoint union of a circle and a cylinder = coexistence of a stable equilibrium with infinity-infinity phase orbits for the same h and the same c (centre SE and phase curves 4 in Fig. 9).
- disjoint union of torus and cylinder = coexistence of quasiperiodic and periodic phase orbits with infinity-infinity phase orbits for the same h and the same c (curves 3 and 4, respectively, in Fig. 9).
- union of torus and cylinder with a common circle = the homoclinic orbit H generated by the saddle UE around the centre SE, coexisting with the orbits 2 (UE-infinity) and $2'$ (infinity-UE) in Fig. 9. The common circle is the saddle UE.

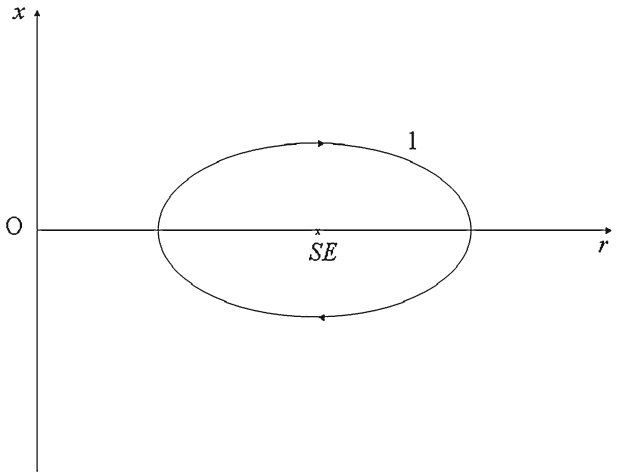

Fig. 7 The phase portrait in the cases $h < 0$ (for any c) and $h = 0, c \neq 0$

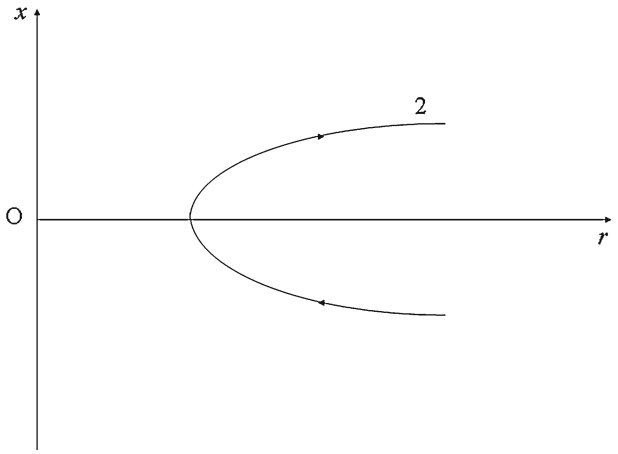

Fig. 8 The phase portrait in the case $h \geq 0, c = 0$

To draw Figs. 7, 8, and 9, we considered three separate situations: $h < 0, h = 0, h > 0$, and, for each situation, we made c^2 increase from zero to higher and higher values (e.g., [6]).

Consider the negative-energy case

For the case of zero angular momentum, the equilibrium *SE* represents a stable rest of the particle with respect to the centre. The curves 1 represent radial librations: the particle moves rectilinearly back and forth between two finite limit distances with respect to the centre.

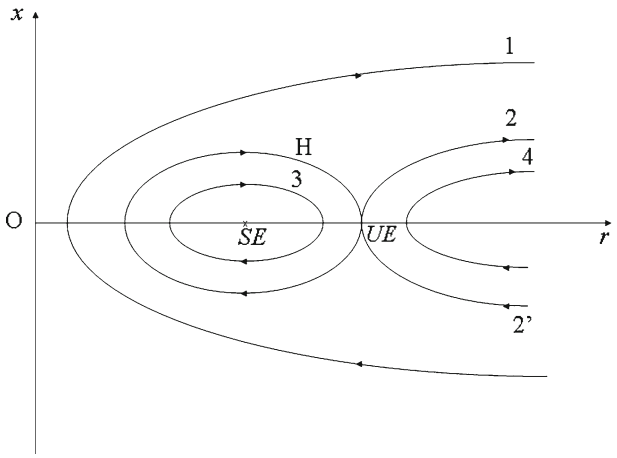

Fig. 9 The phase portrait in the case $h > 0, c \neq 0$

For the case of nonzero angular momentum, the equilibrium *SE* represents a stable circular orbit. The curves 1 represent either quasiperiodic orbits (which fill densely an annulus and never close), or genuine periodic orbits (which close after a finite number of rotations). We have to remark that in this case the set of initial conditions that lead to the phase curves 1, and the set of initial data that lead to periodic solutions is of zero Lebesgue measure (hence improbable), whereas the set of initial data that lead to quasiperiodic solutions is of positive Lebesgue measure.

Consider the zero-energy case

The translation of the phase portrait presented in Fig. 8 in terms of physical motion is very simple. Curves 2 represent radial capture-escape orbits: the particle comes rectilinearly from infinity, stops at a finite distance from the centre, then tends back to infinity. The asymptotic velocity at infinity is zero.

For the case of nonzero angular momentum, the phase portrait is identical to the one presented in Fig. 7. The equilibrium SE represents a stable circular orbit, while the curves 1 represent either quasiperiodic orbits, or periodic orbits.

Consider the positive-energy case

For $c = 0$ the phase portrait is illustrated in Fig. 8: only unbounded phase trajectories are represented by the curves 2. The translation of the respective phase portrait in terms of physical motion is exactly the same as in the zero-energy case. Curves 2 represent radial capture-escape orbits: the particle comes rectilinearly from infinity, stops at a finite distance from the centre, then tends back to infinity. The only difference that appears in the case $h > 0$ as compared to the case $h = 0$ is that the asymptotic velocity at infinity is no more zero (parabolic), but positive (hyperbolic).

For nonzero c, Fig. 9 exhibits a much more rich phase-space structure.

We shall interpret all these phase curves in terms of physical motion.

- The equilibrium SE represents a stable circular orbit around the centre.
- The equilibrium UE represents an unstable circular orbit around the centre, having a radius greater than the one of the stable circular orbit.
- The homoclinic curve H characterizes an orbit that ejects asymptotically from the unstable circular orbit, reaches a finite distance, then tends back asymptotically to the same unstable circular orbit. The physical motion on the homoclinic orbit is spiral.
- The curves 1 represent spiral capture-escape orbits, which approach the centre closer than the distance of the stable circular orbit.
- The curves 2 represent escape spiral orbits that eject asymptotically from the unstable circular orbit and tend to infinity with positive asymptotic velocity.
- The curves $2'$ represent capture spiral orbits that come from infinity (with a positive asymptotic velocity) and tend to the unstable circular orbit.
- The curves 3 characterize quasiperiodic orbits (which fill densely an annulus and never close) and periodic orbits (which close after a finite number of rotations). Within the set of initial conditions that lead to the phase curves 3, the set of initial data that lead to periodic solutions is of zero Lebesgue measure (hence improbable), whereas the set of initial data that lead to quasiperiodic solutions is of positive Lebesgue measure.
- The curves 4 represent spiral capture-escape orbits, whose minimum distance from the centre is farther than the distance of the unstable circular orbit.

To prove the spiral character of the motion on the homoclinic orbit and on the orbits corresponding to the phase curves 1, 2, $2'$, 3, and 4, see, for instance [1], or [9], who proved this in a different context.

9 Concluding remarks

To point out some important and unusual characteristics of the two-body problem associated to our generalized Lennard-Jones-type potential, we mention:

- The existence of stable rest (for the negative-energy level, and for zero angular momentum).
- The existence of radial librations (for the same case of negative-energy level and zero angular momentum).
- The existence of radial capture-escape motion (for non-negative-energy levels, and for zero angular momentum). We can call this the slingshot effect, or the elastic-barrier effect.
- The existence of bounded orbits for non-negative-energy levels.
- The co-existence (for the same energy level, and for the same angular momentum) of wholly different orbits: quasiperiodic (and periodic) and capture-escape, stable circular and capture-escape, and so forth. In such co-existence situations (for the same h and for the same c), the type of orbit is decided by the initial distance of the particle from the centre.
- The existence of a homoclinic orbit for an open set of initial conditions.

Lastly, we have to emphasize the important role of the angular momentum. It generates two bifurcations, as c is zero or nonzero, between the phase planes for $h = 0$, and between the phase planes for $h > 0$ (see the corresponding figures).

References

1. F.N. Diacu, A. Mingarelli, V. Mioc, C. Stoica, in *The Manev two-body problem: quantitative and qualitative theory*, ed. by R.J. Agarwal Dynamical Systems and Applications, World Scientific Series in Applicable Analysis, vol. 4. (World Scientific, Singapore, 1995), pp. 213–227
2. M.V. Hirsch, Differential Topology (Graduate Texts in Math., vol. 33) Springer (1976)
3. J.E. Lennard-Jones, Cohesion. Proc. Phys. Soc. **43**, 461–482 (1931)
4. R. McGehee, Triple collision in the collinear three-body problem. Invent Math. **27**, 191–227 (1974)
5. V. Mioc, M. Stavinschi, On singularities of particle dynamics in quasihomogeneous fields: A first insight. Phys. Scripta **65**, 193–199 (2002)
6. V. Mioc, E. Popescu, N.A. Popescu, Phase-space structure in Lennard-Jones-type problems. Rom. Astron. J. Suppl. **18**, 129–148 (2008)
7. V. Mioc, E. Popescu, N. A. Popescu, Groups of symmetries in Lennard-Jones-type problems. Rom. Astron. J. **18**, 151–166 (2008)
8. D.G. Saari, Regularization and the artificial Earth satellite problem. Celest. Mech. **9**, 55–72 (1974)
9. C. Stoica, V. Mioc, The Schwarzschild problem in astrophysics. Astrophys. Space Sci. **249**, 161–173 (1997)